Real Measurements and Evaluation of the Influence of Atmospheric Phenomena on FSO Combined with Modulation Formats

Jan Latal, Lukas Hajek, Ales Vanderka, Jan Vitasek, Petr Koudelka, Stanislav Hejduk

Abstract— **The influence of atmospheric environment is fundamental for Free-Space Optical link (FSO). The atmosphere can significantly degrade the communication quality of FSO up to so low received power/RSSI level that it can lead to the loss of communication. For this reason, authors used a professional weather station built on site of FSO link for measurement of real atmospheric conditions such as wind speed, temperature, relative air humidity, air pressure and solar radiation. Random changing of these atmosphere parameters creates atmospheric turbulences, absorption and dispersion centers. It is necessary to specify the value of refractive index structure parameter C_n^2 because it determines the influence of atmosphere on the FSO. The first part of this article includes the theoretical calculation of C_n^2, there are used two models PAMELA and Macroscale-Meteorological model. The evaluation of the atmospheric influences and the RSSI value of received power level and also simulation of different types of modulation formats OOK-RZ, OOK-NRZ and BPSK in Optiwave is integral part of this article.**

Index Terms— **atmospherics, eMOS, FSO, modulation format, MOS, PAMELA.**

I. INTRODUCTION

FSO links are used a long time for their advantages in terms of use for communication in the unlicensed band, high security level and simple and fast installation. The FSO began to be extensively used in the context of increasing transmission speed for last mile networks, there was needed a system with a higher capacity in comparison with conventional radio waves communication systems. Increase of the transmission speed and reliability of FSO link is largely given by the type of modulation format, which is used for communication [1]. The most commonly used modulation format is OOK (On Off Keying) in variants RZ (Return to

Zero) and NRZ (Non-Return to Zero) [2]-[6]. In comparison of the FSO and RF system, the FSO is less affected by rain and snow, but atmospheric turbulence and fog dramatically affect the data transmission. Therefore in areas with dynamic weather changes there began to be used links that combines the advantages of FSO and RF. Disadvantage, which greatly reduces deployment and utilization of FSO systems, is then the atmosphere used as a transmission environment [7].

The atmosphere is dynamic and chaotic transmission medium, where the refractive index of air fluctuates during the day, especially at the turn of the day and night. Furthermore, the fluctuations of refractive index are related to wind velocity, roughness of the earth's surface, amount of solar radiation, rainfall, air pressure, density and composition of the air. The intensity of these fluctuations is described by the refractive index structure parameter C_n^2. For the theoretical calculation of refractive index structure parameter there can be used basic mathematical models obtained from empirical study of the influence of the atmosphere on the refractive index structure parameter. These models are known as horizontal models and include the PAMELA model based on the Monin-Obhukov similarity theory (MOS) and Macroscale-Meteorological model based on global meteorological data released by the U.S. Army Night Vision Laboratory. In comparison of these two models, PAMELA model is far more difficult to re-computing performance and includes more parameters. Macroscale-Meteorological model is especially based on special weight function of relative part of day [8]-[13].

The location of measurement and used devices are also described as part of this article. The following chapters describe the theoretical background of mathematical models used to evaluation of the atmospheric effects on the FSO link.

II. DESCRIPTION OF THE MEASURED AREA, USED EQUIPMENT AND MEASURED VALUES

The data were analyzed during the month of April 2015 (1st–15th). These days were chosen due to the completeness of the data and also due to the development of RSSI (Received Signal Strength Indicator) value in each day, because the RSSI value fluctuated approximately within the same range. It was considered that in this month there were very few dispersion centers, which would be appreciably showed on the RSSI diagram.
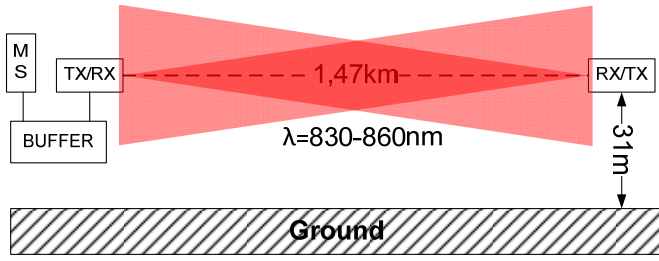
Fig. 1. Basic scheme of FSO system and MS (Meteorological station).

A. Description and measurement of the FSO

Measurement of the RSSI was realized on the installed FSO link in the premises of the VSB–Technical University of Ostrava and on the observatory pylon of Johan Palisa. This is a professional optical link type TS5000G from the MRV. The total length of the optical path was 1.47 km. The FSO heads use as a sources of light radiation three infrared lasers which works at $\lambda = 830$–860 nm, beam divergence was 2 mrad, total power of the optical head was 140 mW (2x40 mW and 1x60 mW). The beam width on the receiver side was 2.94 m. Transmitting lens diameter was 6 cm and receiving lens diameter was 20 cm. The FSO heads include APD diode (sensitivity -33dBm) for detection of the optical signal. The maximum bit rate of the FSO was 1.25 Gbit/s. Azimuth defined by the manufacturer for optical link TS5000G is 107.26°. The basic circuit diagram FSO is shown in Fig. 1. The FSO link transmits periodically a sequence of bits and measures value of the received signal strength indication RSSI. The RSSI is recorded in 60 seconds intervals.

III. MATHEMATICAL MODELING OF THE REFRACTIVE INDEX STRUCTURE PARAMETER C_n^2

Two mathematic models were used for calculation of the refractive index structure parameter C_n^2. The first was PAMELA model which provides estimates of C_n^2 within the surface boundary layer. The required inputs are latitude, longitude, date, time of day, percent cloud cover and terrain type, as well as single measurement of atmospheric temperature, air pressure and wind speed. With the derivation of the basic equation for calculating the refractive index (1) it can be obtained equation for the refractive index structure parameter C_n^2 [7], [11], [13]:

$$\Delta n = \frac{77.6 \times 10^{-6} \times P_a}{T} \times \left(1 + \frac{7.52 \times 10^{-3}}{\lambda^2}\right). \quad (1)$$

By modifying this equation, where λ represents the wavelength of the radiation light source, T=288°K, P_a=1013 hPa, we obtain follow equation:

$$C_n^2 = \frac{b \times K_h}{\varepsilon^{\frac{1}{3}}} \times \left(\frac{\partial n}{\partial h}\right)^2, \quad (2)$$

where b is a constant commonly approximated by 2,8. If we ignore the small contributions to the total differential from fluctuations in atmospheric pressure, we can differentiate (1) with respect to the potential temperature θ and by using next equation (more in [7] or [13]) with ignoring small contributions due to wavelength hit follows that [7], [11], [13]:

$$\frac{\partial n}{\partial h} \approx \frac{\partial n}{\partial \theta} \frac{\partial \theta}{\partial h} \cong \frac{(-77.6 \times 10^{-6} \times P_a) \times T_* \Phi_h \times \left(\frac{h}{L}\right)}{k_\upsilon \times h \times T^2}, \quad (3)$$

where k_υ is von Karman's constant taken to be 0,4, T_* is characteristic or scaling temperature, Φ_h is dimension less temperature gradient, L is Monin-Obukhov length and u_* is friction velocity.

The other model is based on the Macroscale-Meteorological model and it carried out by the U.S. Army Night Vision Laboratory. This model is based on standard meteorological parameters measured over the world. It is also based on the concept of temporal hours or relative part of day. Relations between C_n^2 and th (temporal hour) parameter led to construction of weight function. Values of th are obtained in following ways [8]:

1. one th is obtained by subtraction the hour of sunrise from the sunset and dividing by 12.
2. the current th is obtained by subtraction the hour of sunrise from current hour and dividing by the value of 1 th.

$$C_n^2 = 3,8 \times 10^{-14} W + f(T) + f(U) + f(RH) - 5,3 \times 10^{-13}, \quad (4)$$

$$f(T) = 2 \times 10^{-15} \times T, \quad (5)$$

$$f(U) = -2.5 \times 10^{-15} U + 1.2 \times 10^{-15} U^2 - 8.5 \times 10^{-17} U^3, \quad (6)$$

$$f(RH) = -2.8 \times 10^{-15} RH + 2.9 \times 10^{-17} RH^2 \quad (7)$$
$$-1.1 \times 10^{-19} RH^3$$

where W is temporal hour weight, T is air temperature in degrees of Kelvin, RH is relative humidity in (%) and WS is wind speed (m/s) [2]. This model has some limitations due to the weather conditions, for which it is valid. According to the theory [9] is a basic MOS model limited by temperature range of 9–35°C, relative humidity range 14–92% and wind speed range of 0–10 m/s. The MOS model has certain limitations therefore it is not suitable e.g. for coastal areas where it can be assumed a higher air velocity and also higher air humidity. For this reason, the original MOS model was modified on the new version eMOS (extended Macroscale Meteorological Model):

$$C_n^2 = 3.8 \times 10^{-14} W + \frac{A}{\exp(T)} \times 10^{-14} + f(U) + \quad (8)$$
$$+ f(RH) - 4.45 \times 10^{-14}$$

$$f(U) = 2.58 \times 10^{-14} U, \quad (9)$$

$$f(RH) = -6.797 \times 10^{-15} RH. \quad (10)$$

These equations (9) and (10) are valid in case that the area is covered by vegetation. The theory [9] describes an alternative variant of (9) and (10), which are mainly

designated for the mountainous areas. This model has its limitations for wind speed of range 5–10 m/s and relative humidity 92–100%.

IV. MEASUREMENT OF CLIMATIC EFFECTS

The weather station Davis Vintage Pro2 was used for measurement of meteorological data. This weather station is installed in close proximity to the FSO head on the roof of the main building of VSB–Technical University of Ostrava. In addition to the values of wind speed, temperature, pressure, relative humidity and solar radiation, the weather station is also capable to measure the wind direction and rainfall. Separate data were read in minute interval in time period. During the measurement of climatic influences a sensor failure occurred in 10th and 11th day of measuring due to electric energy failure. Due to this failure the days 10th April 2015 and 11th April 2015 were removed from subsequent calculations.
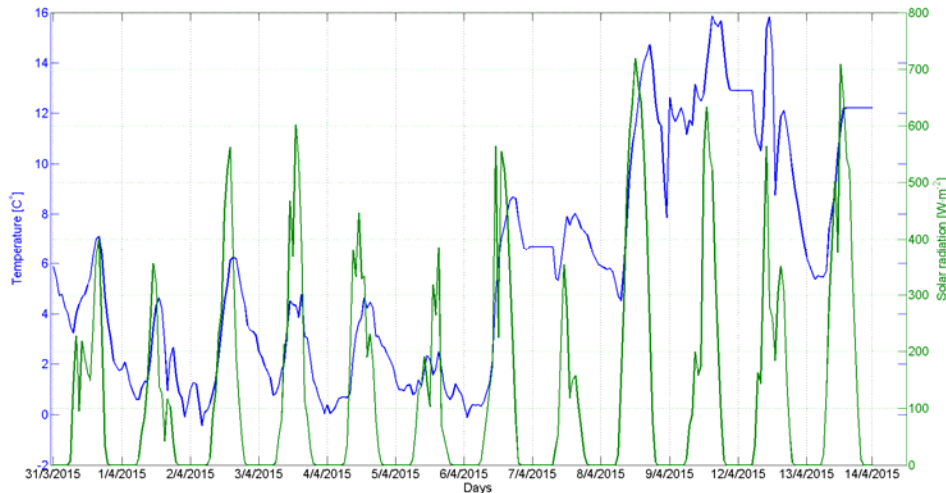

Fig. 2. Measurement of temperature and solar radiation in period 1st to 14th April 2015.
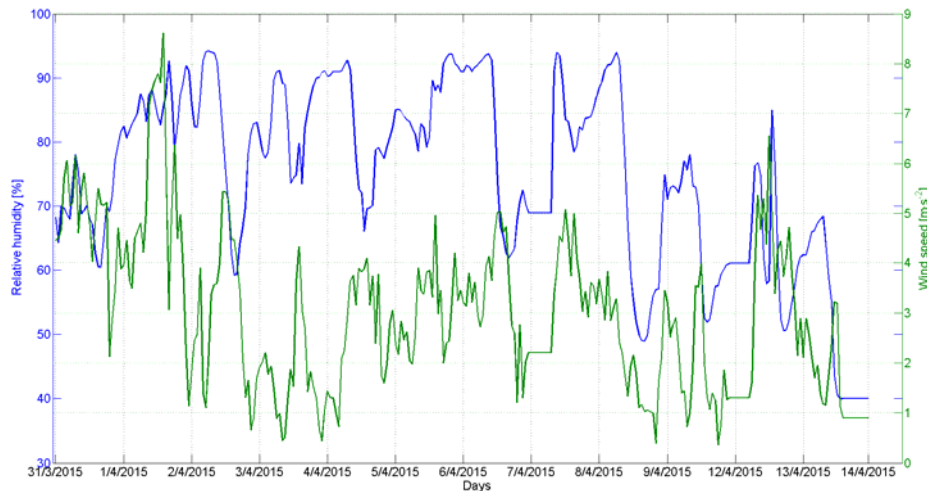

Fig. 3. Measurement of relative humidity and wind speed in period 1st to 14th April 2015.

Figure 2 shows measured values of temperature gradient in correlation with solar radiation for monitored period. It is clear obvious from Fig. 2 that the unambiguous trend of temperature increasing with increasing solar radiation. In period of 1st–8th April 2015 the relative humidity was around 90 % in night hours and up to 70 % in day hours. In period of 9th to 14th April 2015 the mean value of relative humidity decreased which is related to increasing of outdoor air temperature, see Fig. 2. The maximal wind speed was 9 m/s which answers to limit cases of wind speed for MOS and eMOS models . The last Fig. 4 in this section shows behavior of atmospheric pressure which increased from the start of measurement to maximal value around 1030 hPa. The behavior of RSSI [-] level of FSO link periodically increased and decreased approximately from 250 to 530. Notice that occurred stationary increasing of RSSI values from 3rd April 2015. Also other figures show change of atmosphere behavior with air temperature increasing.
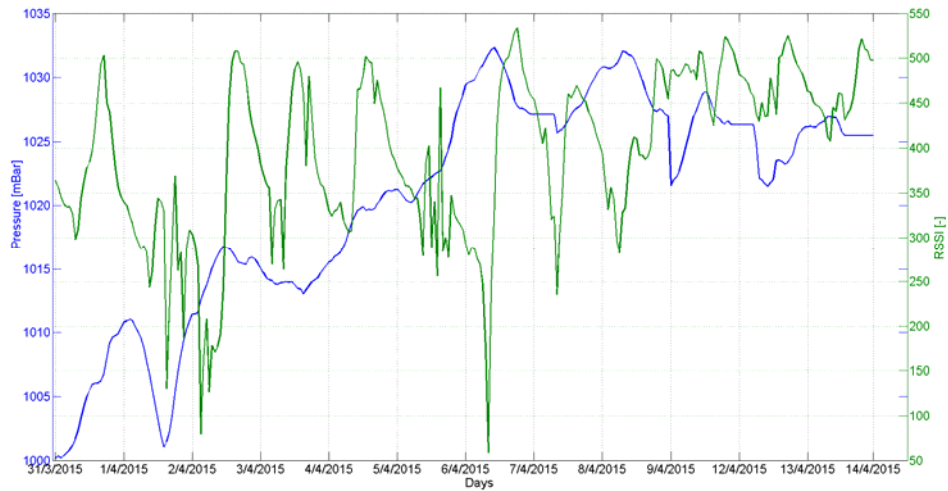
Fig. 4. Measurement of voltage level RSSI and atmospheric pressure in period 1st to 14th April 2015.

V. CALCULATION OF REFRACTIVE INDEX STRUCTURE PARAMETER C_n^2

According to the theory described in III. section the calculations of models PAMELA, MOS and eMOS were done in software Matlab. These calculations went from measured data which were obtained in period 1st to 14th April 2015. These data are used as variables which enable to calculate C_n^2 according to models PAMELA, MOS and eMOS. The final calculation is displayed in Fig. 5a, 5b and 5c, where the x-axis represents minutes of one day and y-axis shows values of the refractive index structure parameter C_n^2. The calculations of separate minutes are represented by grey crosses. For each minute, the 12 calculations were done in our cases and from these 12 values in each minute the arithmetic mean (red line) was calculated. Fig. 5d shows the final comparison of three models.
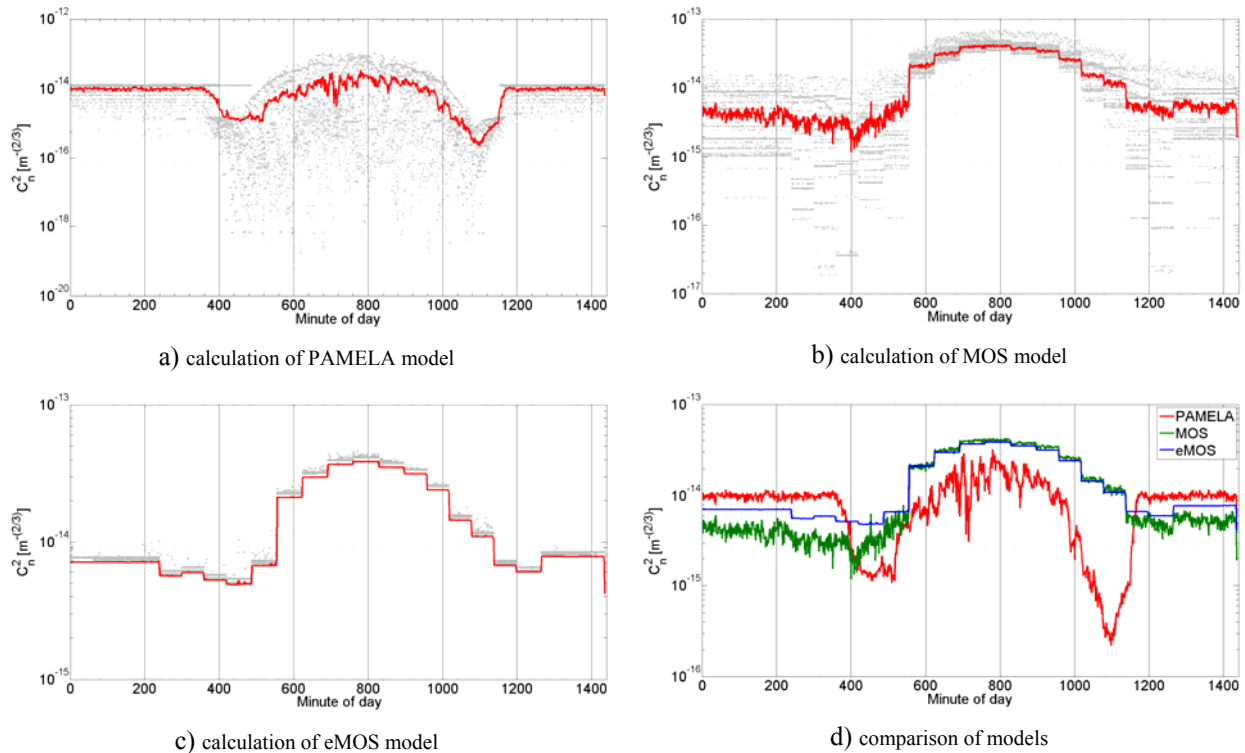

a) calculation of PAMELA model

b) calculation of MOS model

c) calculation of eMOS model

d) comparison of models

Fig. 5. Calculation of refractive index structure parameter for mean values of atmospherical conditions in period 1st to 14th April 2015.

VI. SIMULATION OF INFLUENCE OF ATMOSPHERIC PHENOMENA ON FSO IN OPTIWAVE SYSTEM

Optiwave OptiSystem software ver. 11 was used for simulation of the influence of atmospheric conditions on the FSO link. We selected mostly used modulation formats RZ, NRZ and BPSK in FSO communications (see Fig. 6) for simulation of the influence of atmospheric phenomena on the quality of communication. The modulation formats affect important parameters such as bandwidth and energy efficiency, which affect overall system performance. The main goal of modulation formats is increasing spectral/power efficiency and reducing sensitivity to fluctuation of received power [14], [15]. The modulation of the optical beam is provided in optical area by Mach-Zender modulator, see Fig. 6.
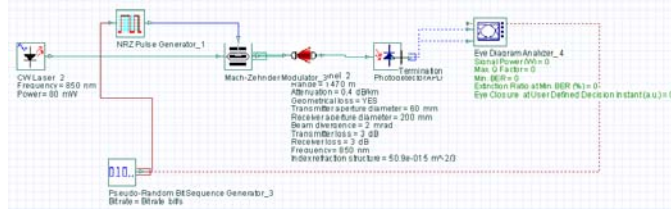

Fig. 6. Simulation scheme of the influence of atmospheric phenomena on FSO link in Optiwave system.

The simulations were set to correspond to the real FSO link, which is placed in the campus. The OOK (On-Off-Keying) modulation format is the most commonly used in commercial terrestrial FSO communications. Advantage of this format is resistance to nonlinearities of the laser and an external modulator. However, this format is much more sensitive to turbulence and other disturbances which lead to fluctuation of received optical power. We can reduce this fluctuation by replacing the decision-making level with adaptive decision-making level. The OOK modulation format can be used with non-return to zero (NRZ) or return to zero (RZ) link code. For OOK-NRZ modulation format the BER can be defined as [2], [7], [15]:

$$BER_{(OOK-NRZ)} = \frac{1}{2} \cdot erfc \cdot (\frac{1}{2\sqrt{2}} \sqrt{SNR}) , \qquad (11)$$

where is *erfc* (error function also called the Gaussian error function) and *SNR* is signal-to-noise ratio defined in dB units. For OOK-RZ format the pulse duration is shorter for "1" thereby the energy efficiency increases, but RZ requires larger bandwidth than NRZ. The BER of OOK-RZ can be defined as [2], [7]:

$$BER_{(OOK-RZ)} = \frac{1}{2} \cdot erfc \cdot (\frac{1}{2} \sqrt{SNR}) . \qquad (12)$$

The BPSK (also sometimes called Phase Reversal Keying (PRK), or 2PSK) is the simplest form of PSK (Phase Shift Keying) modulations. It uses two phases with difference of 180°. It does not exactly matter where the constellation points are positioned. This modulation is the most robust of all the PSK modulations nevertheless it takes the highest level of noise or distortion which could lead to an incorrect decision.

However, it only modulates 1 bit/symbol thereby it is unsuitable for high data-rate applications. BPSK has variety of applications in digital communications systems such as the wireless LAN standard, IEEE 802.11, digital modems, wireless telephone networks etc. BPSK modulation format is functionally equivalent to 2-QAM (Quadrature Amplitude Modulation) modulation. BER for BPSK can be defined as [2], [7]:

$$BER_{(BPSK)} = \frac{1}{2} \cdot erfc \cdot (\frac{\sqrt{SNR}}{\sqrt{2}}) . \qquad (13)$$

Values of refractive index structure parameter calculated according real data were successively entered in OptiSystem, the simulations calculated the BER and the eye diagrams. Figure 7 shows the calculated dependence of the BER on the refractive index structure parameter. The refractive index structure parameter values were entered from 10^{-17} to 10^{-12} with logarithmic increase.

We highlighted the area from $2.21 \cdot 10^{-16}$ do $4.27 \cdot 10^{-14}$ in Fig. 7, these values correspond to the maximum and minimum value of the refractive index structure parameter calculated by models. The expected increasing of BER is reflected in this area that shows the logarithmic character of BER. However, computational model presents particular and mistaken behavior in the area around $4 \cdot 10^{-14}$, when BER begins decline with increasing turbulence error rate. This behavior is contrary to the logical assumption and it can be considered as an error caused by an internal algorithm program.
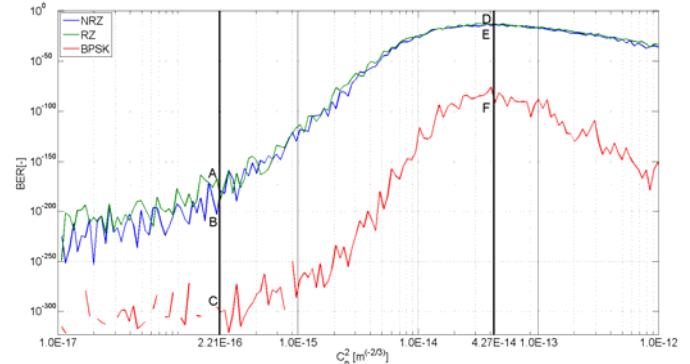

Fig. 7. Simulation of depending of refractive index structure parameter on the BER for modulation formats NRZ, RZ and BPSK.

Fig. 7 shows the points of intersection of the individual charts with the limit values of the refractive index structure parameter. The eye diagrams were monitored for these limit states. Fig. 8a)–8f) show individual eye diagrams for the marked points A-F. The eye diagrams and the characteristics of the waveforms on Fig. 7 show that the most resistant modulation format is BPSK for the examined area. The other modulation formats RZ and NRZ exhibit small deviation. NRZ and RZ modulation at limit values clear reflect increasing of symbol errors ISI (Intersymbol Interference) and eye closure. From simulated data for BPSK modulation format it can be also observed that the marked red curve of *Q factor* is unchanged at the minimum and maximum influence values of the refractive index structure parameter. Transmission speed of optical head for the simulation was set to 1.25 Gb/s, which corresponds to real value of the optical head MRV TS5000G [16].

a) RZ

d) RZ
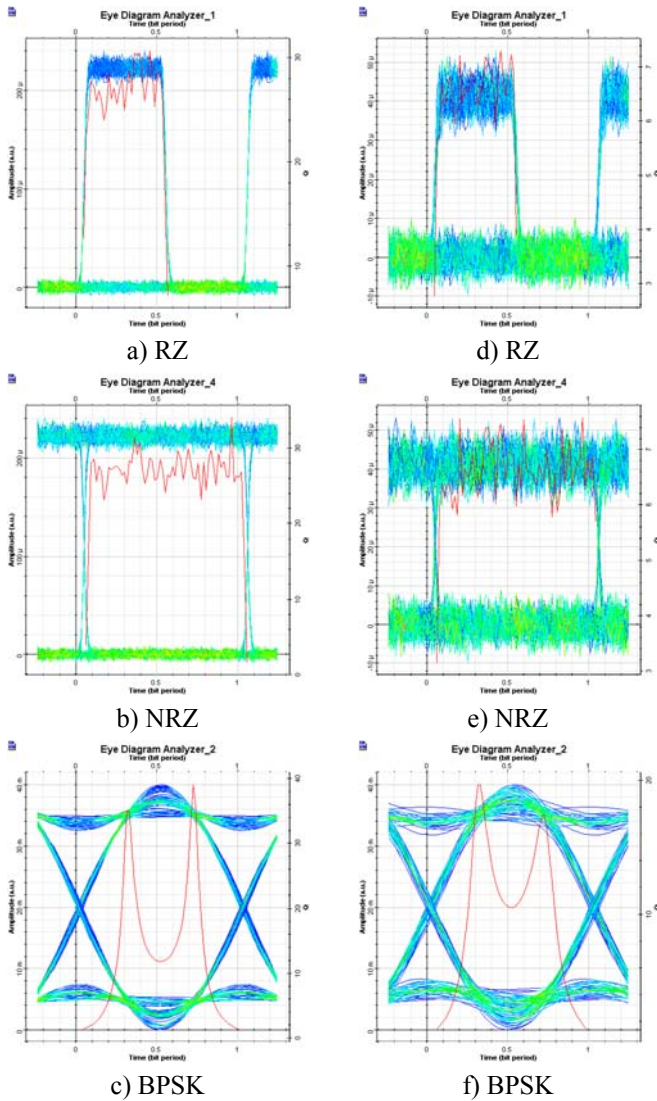

b) NRZ

e) NRZ

c) BPSK

f) BPSK

Fig. 8. Eye diagrams for dependency between BER and refractive index structure parameter.

Development of BER with regards to chosen type of modulation format and refractive index structure parameter for models PAMELA, MOS and eMOS is showed in Fig. 9–11. Good results could by seen for modulation format BPSK from simulations and development of BER parameter (Fig. 8 c, f). This behavior is not in the case of RZ (Fig. 8 a, d) or NRZ (Fig. 8 b, e) modulation format, increasing of BER is more significant for these modulations. In this case interruption of communication channel could occur due to higher values of BER.
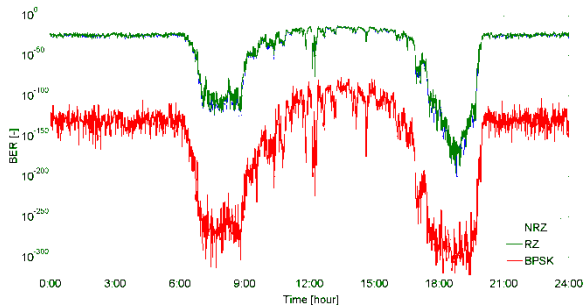

Fig. 9. BER simulation for refractive index structure parameter computed by PAMELA algorithm.
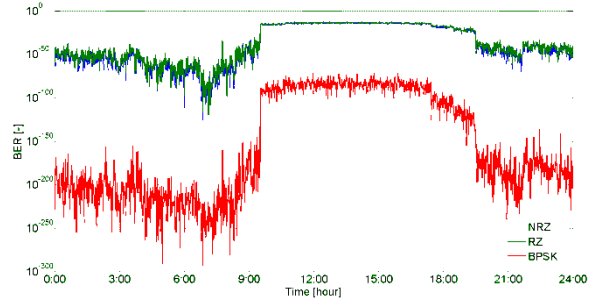

Fig. 10. BER simulation for refractive index structure parameter by MOS algorithm.
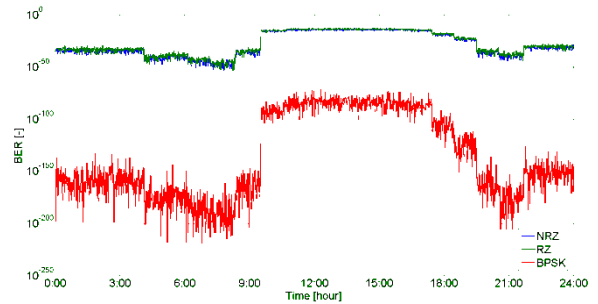

Fig. 11. BER simulation for refractive index structure parameter computed by eMOS algorithm.

The last simulation is calculation of maximal range of FSO link for minimal and maximal C_n^2 value. We simulated the range for modulations RZ, NRZ and BPSK with the same BER=10^{-12}. The attenuation coefficient of atmosphere was set to 0.4 dB/km. Table I summarizes the simulated results for maximal range of FSO link. It is obvious that maximal range of FSO link could be achieved by using BPSK modulation.

VII.   CONSLUSION

Within this article the team of authors focused its attention to the area of atmospheric influence on Free-Space-Optics. Based on real measured values of atmospheric environment three models of refractive index structure parameter (PAMELA, MOS and eMOS) were computed. Each model uses different principles for calculation of the C_n^2 which is reflected especially during sunset and sunrise, when PAMELA model has the lowest level of turbulence compared to MOS

TABLE I
SIMULATION OF MAXIMAL RANGE OF FSO LINK

α=0.4dB/km, BER=10^{-12}	Refractive index structure parameter		
Modulation formats	$C_n^2 = 10^{-14}$	$C_n^2 = 10^{-15}$	$C_n^2 = 10^{-16}$
RZ	1550m	1700m	2900m
NRZ	1500m	1600m	2800m
BPSK	2700m	2800m	4500m

and eMOS. These models were then correlated with BER for different modulation formats in our case RZ, NRZ, and BPSK. With regards to real atmospheric measurement, the BPSK modulation showed good error-resistant in turbulent condition in comparison to RZ and NRZ modulation.

REFERENCES

[1] R. Ramirez-Iniguez, S. M. Idrus, Z. Sun, *Optical Wireless Communications: IR for wireless connectivity*, USA: CRC Press, 2008.

[2] S. Arnon, J. Barry, G. Karagiannidis, R. Schober, M. Uysal, *Advanced Optical Wireless Communication Systems*, UK: Cambridge University Press, 2012.

[3] A. Vaderka, L. Hajek, J. Latal, J. Vitasek and P. Koudelka, "Design, simulation and testing of the OOK NRZ modulation format for free space optic communication in a simulation box," *Advances in Electrical and Electronic Engineering*, vol. 12, pp. 604–616, Dec. 2014.

[4] W. O. Popoola and Z. Ghassemlooy, "BPSK subcarrier intensity modulated free space optical communications in atmospheric turbulence," *Journal of Lightwave Technology*, vol. 27, pp. 967–973, April 2009.

[5] J. Li, J.Q. Liu and D.P. Taylor, "Optical communication using subcarrier PSK intensity modulation through atmospheric turbulence channels,"

[6] B. Barua and D. Barua, "Evaluate the performance of FSO communication link with different modulation technique under turbulent condition," in *14th International Conference on Computer and Information Technology (ICCIT)*, Dhaka, 2011, pp. 191–196.

[7] A. K. Majumdar and J. C. Ricklin, *Free-space laser communications*, USA: Springer, 2008.

[8] N. S. Kopeika and J. C. Ricklin. *A system engineering approach to imaging: Principles and advances*. USA SPIE Optical Engineering Press, 1998.

[9] S. Bendersky, N. S. Kopeika, and N. Blaunstein, "Atmospheric optical turbulence over land in Middle East coastal environments: Prediction modeling and measurements," *Applied Optics*, vol. 43, pp. 4070–4079. Jul. 2004.

[10] S. Doss-Hammel, E. Oh, J. C. Ricklin, F. D. Eaton, G. Ch. Gilbreath, D. Tsintikidis, J. C. Ricklin and D. G. Voelz. "A comparison of optical turbulence models," in *Proceedings of SPIE, Free-Space Laser Communications IV*, vol. 5550, Denver, 2004, pp. 236–246.

[11] A. Tunick, "C_n^2 model to calculate the micrometeorological influences on the refractive index structure parameter," *Environmental Modelling & Software*, vol. 18, pp. 165–171, Mar. 2003.

[12] N. Blaunstein, S. Arnon, A. Zielberman and N. S. Kopeika. *Applied aspects of optical communication and LIDAR*, USA: CRC Press, 2009.

[13] Z. M Jacobson, *Fundamentals of atmospheric modeling*, UK: Cambridge University Press, 2005.

[14] R. Martinek, J. Zidek, and K. Tomala. "BER measurement in software defined radio systems," *Przegląd Elektrotechniczny*, vol. 89, pp. 205–210, Feb. 2013.

[15] T. Y. Elganimi, "Studying the BER Performance, Power- and Bandwidth-Efficiency for FSO Communication Systems under Various Modulation Schemes," in *IEEE Jordan Conference on Applied Electrical Engineering and Computing Technologies (AEECT)*, Amman, 2013, pp. 1–6.

[16] http://www.mrvfso.com/model/ts5000/ (assessed 13.01.2016)

IEEE Transaction on Communication, vol. 55, pp. 1598–1606, Aug. 2007.